SU(2) flux distributions on finite lattices

Yingcai Peng and Richard W. Haymaker

Department of Physics and Astronomy,
Louisiana State University, Baton Rouge, Louisiana 70803-4001

We studied SU(2) flux distributions on four-dimensional Euclidean lattices with one dimension very large. By choosing the time direction appropriately we can study physics in two cases: one is finite volume in the zero-temperature limit, another is finite temperature in the intermediate to large volume limit. We found that for cases of $\beta > \beta_c$ there is no intrinsic string formation. Our lattices with $\beta > \beta_c$ belong to the intermediate volume region, and the string tension in this region is due to finite volume effects. In large volumes we found evidence for intrinsic string formation.

I. INTRODUCTION

There are two complementary ways to obtain approximate solutions of strong-coupling QCD. One is to take three-space to be a finite-volume torus and obtain semi-analytic solutions [1–3] of an effective Hamiltonian. The second is via lattice simulations. Confinement can be studied by each method in limited domains. In small physical volumes the fields are very rigid and the problem can be treated using a variational method applied to a small number of dynamical variables. In this domain the string tension is found to be zero. This result is consistent with asymptotic freedom since only short-wavelength modes occur. At intermediate volumes there is a clear signal for string tension, and further that it is a consequence of a tunneling amplitude between the vacua that are degenerate for small volumes. In this domain, lattice methods are also accessible and are in good agreement for quantities such as glueball masses and string tension. Lattice calculations can take over to study larger volumes where semianalytic methods become prohibitive.

The existence of string tension in finite volumes does not imply confinement. Clearly if the volume is not large enough to allow the fields to spread out, the finite box itself may be responsible for the linearly rising potential energy between quarks. Global studies have left open the question of the volume at which intrinsic confinement takes over [4]. In this paper we look at a local quantity, the flux tube profile between static quarks as a function of physical volume in SU(2) lattice gauge theory in order to elucidate this question.

The physical size of the box is characterized by a dimensionless variable

$$z_g \equiv m(0^+)L, \tag{1}$$

where $m(0^+)$ is the lowest glueball mass which is the energy gap or in terms of length it is the inverse of the correlation length. The length L is the linear size of the box. Lüscher studied QCD in a small box, $z_g \leq 1$, with periodic boundary conditions. He derived a low-energy effective Hamiltonian for SU(N) gauge theory in small volumes [1], i.e., $z_g \leq 1$. Subsequently the lowest-energy

levels of SU(2) [2] and SU(3) [5] gauge theories in small volumes were computed by using this Hamiltonian. van Baal and Koller then found that the crucial tunneling between degenerate vacua can be obtained by imposing appropriate nonperturbative boundary conditions on the Raleigh-Ritz trial wave functions [3]. They extended the calculation of the SU(2) glueball masses up to $z_g \approx 5.0$.

Berg and Billoire [4] carried out a thorough study of glueball masses, electric flux states, and string tension for intermediate volumes ($1 \leq z_g \leq 5$). They provided a detailed comparison between their numerical results and the analytic results of van Baal and Koller. They chose lattice sizes $N_a \times N_b^2 \times N_c$, with

$$N_a \leq N_b \ll N_c. \tag{2}$$

By identifying N_c to be the time extent, one can simulate the zero-temperature finite-volume, $N_a N_b^2 a^3$, field theory, with the temperature defined as [6]

$$T_B = \frac{1}{N_c a}, \tag{3}$$

where T_B is called *box temperature* in Ref. [4], and a is the lattice spacing.

Physically, the choice of the time direction is related to interpreting Polyakov loop correlations as the $q\bar{q}$ potential; then the time direction is the one in which the Polyakov loop closes. In our study we follow Berg and Billoire to choose Polyakov loops closed in the N_a direction and their correlations measured along the N_c direction. Then the *physical temperature* is defined to be

$$T_p = \frac{1}{N_a a}. \tag{4}$$

In the coming sections we shall use the physical temperature (T_p) interpretation, so we shall drop the subscript p, i.e., $T = T_p$. In the last section we shall relate this to the box temperature (T_B) interpretation.

After a complete study in the intermediate volume region ($1 < z_g < 5$), Berg and Billoire concluded that they did not find evidence for string formation in this region, but it is expected to occur in larger volumes. The ques-

tion this paper studies is how to understand the string tension measured in intermediate volumes. Is the string tension just due to finite-size effects? Since the string tension was calculated from correlations of Polyakov loops closed in the N_a direction, this can be considered as measuring the potential energy of a $q\bar{q}$ pair in a long rectangular box, with the volume $V = N_b^2 N_c a^3$ and at the finite temperature $T = 1/N_a a$, as shown in Fig. 1. As we know, at high temperatures, $T > T_c$, where T_c is the deconfining temperature, the $q\bar{q}$ is unconfined in the infinite volume limit (N_b, $N_c \to \infty$). However, as the transverse size N_b is made small, i.e., $r/N_b a \geq 1$, one expects the side walls of the box would squeeze the flux lines of the $q\bar{q}$ pair to form a tube although there is no intrinsic string formation in this case, as displayed in Fig. 1. In the following we will present our studies about the $q\bar{q}$ flux distributions which would support the above description.

The remaining parts of this paper are arranged as follows. Section II gives the basic concepts of the flux measurements. Section III discusses the $q\bar{q}$ flux distributions at finite temperatures and finite-volume effects. Section IV discusses the relation between the $q\bar{q}$ flux distributions in a finite box and the string tension in intermediate and large volumes. Finally, Sec. V gives the summary.

II. MEASUREMENTS OF THE FLUX DISTRIBUTIONS

In our study of the SU(2) lattice gauge theory (LGT) we use the standard Wilson action

$$S(U) = \beta \sum_P (1 - \tfrac{1}{2}\mathrm{Tr}U_P), \tag{5}$$

where U_P is the product of link variables around a plaquette, i.e.,

$$U_P(n) = U_\mu(n)U_\nu(n+\mu)U_\mu^{-1}(n+\nu)U_\nu^{-1}(n).$$

We can measure the flux distributions of a $q\bar{q}$ pair by calculating the quantity [7]

$$f_{\mu\nu}(\mathbf{r}, \mathbf{x}) = \frac{\beta}{a^4}\left[\frac{\langle P(0)P^\dagger(\mathbf{r})\square_{\mu\nu}(\mathbf{x})\rangle}{\langle P(0)P^\dagger(\mathbf{r})\rangle} - \langle\square_{\mu\nu}\rangle\right], \tag{6}$$
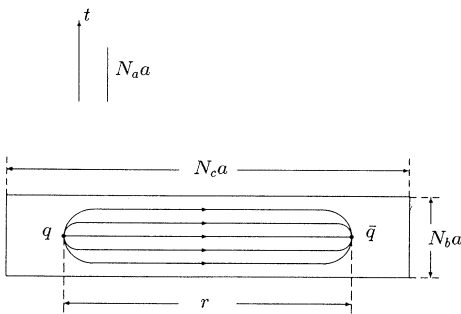

FIG. 1. The $q\bar{q}$ color sources in a long rectangular box. The flux lines between the $q\bar{q}$ pair are confined by side walls and have a flux tube form.

where $P(\mathbf{r}) \equiv \tfrac{1}{2}\mathrm{Tr}\prod_{\tau=1}^{N_a} U_a(\mathbf{r}, \tau)$, is the Polyakov loop closed in the N_a direction and $\square_{\mu\nu} = \tfrac{1}{2}\mathrm{Tr}(U_P)$ is the plaquette variable with the orientation (μ, ν), which has six different values: $(\mu, \nu) = (2, 3)$, $(1, 3)$, $(1, 2)$, $(1, 4)$, $(2, 4)$, $(3, 4)$.

To reduce the fluctuations of the quantity $P(0)P^\dagger(\mathbf{r})\square$, in practical calculations we measure the quantity [7]

$$f'_{\mu\nu}(\mathbf{r}, \mathbf{x})$$

$$= \frac{\beta}{a^4}\left[\frac{\langle P(0)P^\dagger(\mathbf{r})\square_{\mu\nu}(\mathbf{x})\rangle - \langle P(0)P^\dagger(\mathbf{r})\square_{\mu\nu}(\mathbf{x}_R)\rangle}{\langle P(0)P^\dagger(\mathbf{r})\rangle}\right], \tag{7}$$

as the flux distribution instead of Eq. (6), where the reference point $\mathbf{x}_R$ was chosen to be far from the $q\bar{q}$ sources. This replacement does not change the measured average due to the cluster decomposition theorem. The six components of $f'_{\mu\nu}$ in Eq. (7) correspond to the components of the chromoelectric and chromomagnetic fields $(\mathcal{E}, \mathcal{B})$ in Minkowski space, i.e.,

$$f'_{\mu\nu} \to \frac{1}{2}(-\mathcal{B}_1^2, -\mathcal{B}_2^2, -\mathcal{B}_3^2, \mathcal{E}_1^2, \mathcal{E}_2^2, \mathcal{E}_3^2). \tag{8}$$

We then define the total electric energy density to be

$$\rho_{\mathrm{el}} = \frac{1}{2}[\mathcal{E}_1^2 + \mathcal{E}_2^2 + \mathcal{E}_3^2], \tag{9}$$

and the total magnetic energy density

$$\rho_{\mathrm{ma}} = \frac{1}{2}[\mathcal{B}_1^2 + \mathcal{B}_2^2 + \mathcal{B}_3^2]. \tag{10}$$

In the following we will concentrate on studying the total energy and action densities ρ_E and ρ_A, which are the combinations of ρ_{el} and ρ_{ma}. The total energy density is

$$\rho_E = \rho_{\mathrm{el}} + \rho_{\mathrm{ma}}. \tag{11}$$

The total action density is

$$\rho_A = \rho_{\mathrm{el}} - \rho_{\mathrm{ma}}. \tag{12}$$

In our measurements we transformed our flux data from lattice units to physical units by using the scaling relation given by Table I, which was obtained from a similar table in Ref. [8] and we interpolated points in the region $2.22 < \beta < 2.50$. The details of the interpolation process are presented elsewhere [9].

III. FLUX DISTRIBUTIONS AT FINITE TEMPERATURES

It is well known that SU(N) gauge theory has a deconfining phase transition at some finite temperature, T_c

TABLE I. The correspondence of the lattice spacing a and the coupling constant β for SU(2) LGT.

β	2.25	2.28	2.36	2.40
a (fm)	0.1966	0.1785	0.1374	0.1203

[10]. This finite temperature phase transition has been studied extensively in SU(N) LGT. The transition temperature T_c can be determined from Monte Carlo calculations; for example, the critical temperature for SU(2) was determined to be [11]

$$\beta_c = 2.2985 \pm 0.0006 \qquad \text{(for } N_a = 4\text{)}. \qquad (13)$$

The relation between β_c and T_c is $T_c = 1/N_a a(\beta_c)$, as given by Eq. (4). The lattice spacing a is a function of the coupling constant β, such as that of Table I. The phase transition is expected to occur in the infinite volume limit, i.e., N_b, $N_c \to \infty$. In this limit, for $\beta < \beta_c$, the system is in the confined phase; otherwise, it is in the unconfined phase.

We measured the $q\bar{q}$ flux distributions on lattices $N_a \times N_b^2 \times N_c$ with $N_a = 4$, $N_b = 5, 7, 9$, and 11, and $N_c = 65$. Since $N_c \gg N_a$, N_b, as N_b/N_a gets large, we expect the system to approach the infinite volume limit and one should see the two phases. However, for N_b small, that is, N_b satisfying the condition

$$N_b \simeq N_a \qquad \text{and} \qquad N_b a/r \leq 1, \qquad (14)$$

the $q\bar{q}$ pair is in a finite box and one expects finite-volume

effects to be large. In the following we will study the flux distributions with $\beta > \beta_c$ and $\beta < \beta_c$ in various spacial volumes, respectively.

A. Flux distributions with $\beta > \beta_c$

In this case the $q\bar{q}$ system approaches the unconfined phase as the volume becomes large ($N_b \to \infty$). In this phase we expect that there is no string formation. However, for a small volume one expects finite-volume effects to be large.

In Fig. 2 we show some typical results of the energy density ρ_E distributions in the region of $\beta > \beta_c$ ($\beta = 2.40$). They are the flux distributions on the transverse plane midway between the $q\bar{q}$ sources with fixed separation $r = 4a$, and they were measured on lattices of four different spatial sizes $N_b=5, 7, 9, 11$. For N_b small (i.e., $N_b=5, 7$) the transverse plane is the whole lattice. For large N_b ($N_b=9, 11$) the data are truncated on the margins. The signal is lost in the noise beyond the region shown.

From Fig. 2 we can compare the flux distributions in boxes of different transverse size N_b. One can clearly see
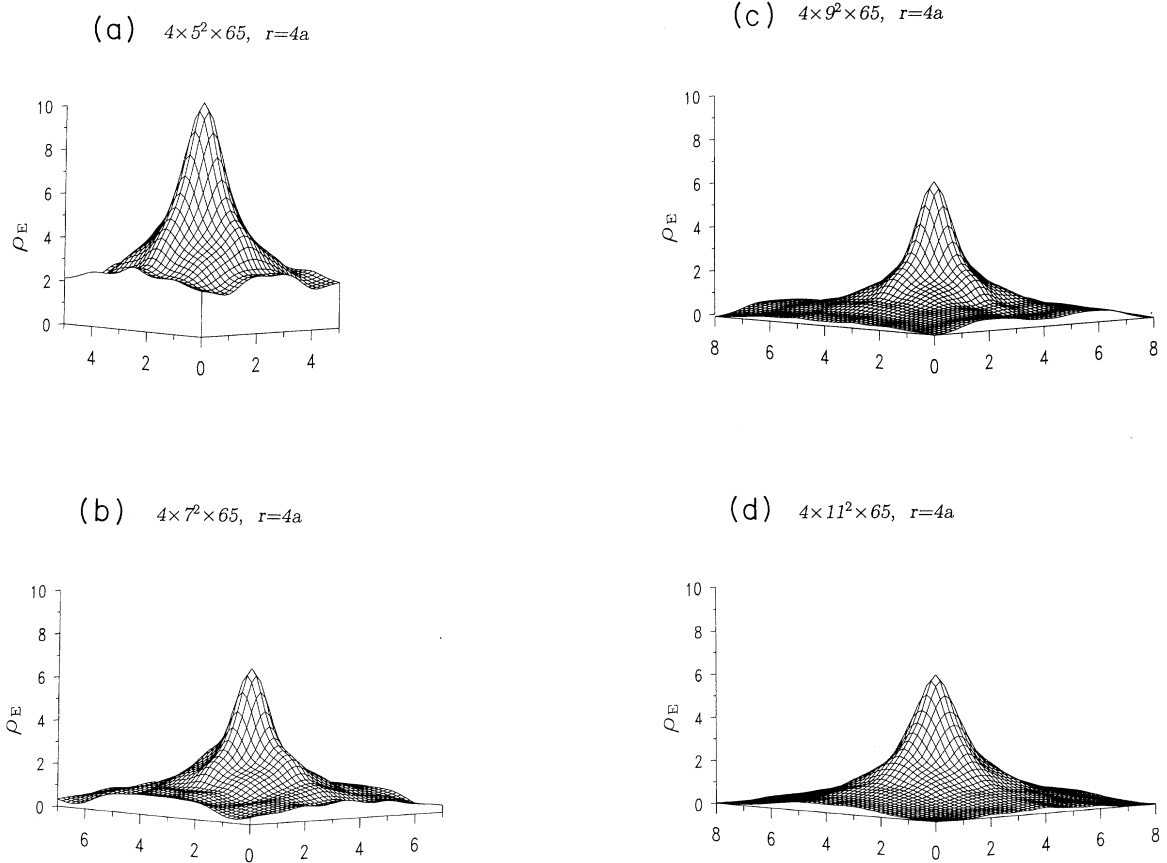
(a) $4 \times 5^2 \times 65$, $r=4a$

(c) $4 \times 9^2 \times 65$, $r=4a$

(b) $4 \times 7^2 \times 65$, $r=4a$

(d) $4 \times 11^2 \times 65$, $r=4a$

FIG. 2. The energy density ρ_E flux distributions in the region of $\beta > \beta_c$ on the plane midway between the $q\bar{q}$ sources of separation $r = 4a$. The flux data were measured on lattices $4 \times N_b^2 \times 65$ with $\beta = 2.40$ for various spatial sizes, (a) $N_b = 5$, (b) $N_b = 7$, (c) $N_b = 9$, and (d) $N_b = 11$. These flux data are measured in the physical unit GeV/fm^3.

for N_b small the flux density ρ_E at the edges of each plane have large values, as shown in Figs. 2(a), and 2(b). This implies that finite-volume effects are significant when N_b is small because in small volumes flux lines of the $q\bar{q}$ sources would be squeezed dramatically by side walls of the box, so the values of ρ_E at edges are large in this case. As we increase the transverse size N_b finite-volume effects become smaller, the flux density ρ_E at edges decrease rapidly to zero, as shown in Figs. 2(c) and 2(d).

Here we want to emphasize that the values of ρ_E at the edges of each plane are not due to the reference point in Eq. (7). In our flux measurement we choose the reference point $\mathbf{x}_R$ far from the $q\bar{q}$ sources, and we find the reference value $\langle P(0)P^\dagger(\mathbf{r})\square_{\mu\nu}(\mathbf{x}_R)\rangle$ in Eq. (7) is consistent with the product $\langle P(0)P^\dagger(\mathbf{r})\rangle\langle\square_{\mu\nu}\rangle$ within errors.

In Table II we list the typical values of flux densities ρ_E, ρ_A at edges of each plane in Fig. 2 and their corresponding errors. From this table one can explicitly see that the values ρ_E and ρ_A at edges decrease rapidly with N_b, as we observed from Fig. 2. However, we also notice that even in cases of large N_b (i.e., N_b=9, 11) the

TABLE II. The typical measured flux density values (errors) of ρ_E and ρ_A in the region of $\beta > \beta_c$ on the edges of the transverse plane midway between the $q\bar{q}$, as shown in Fig. 2. The flux data are in the physical unit GeV/fm^3.

| $r = 4a$ | N_b | $4 \times N_b^2 \times 65$ |
		5	7	9	11
$\beta = 2.40$	ρ_E	2.5 (5)	0.86 (24)	0.11 (18)	0.31 (17)
	ρ_A	17.0 (6)	2.9 (3)	1.5 (2)	1.0 (2)

values of ρ_A shown are nonzero within errors. This may be caused by a number of factors. The edge of the plane is not the boundary of the lattice for cases of N_b=9, 11, the flux values may in fact vanish on the boundary of the lattice, but we did not calculate them there for practical reasons. Also N_b is perhaps not large enough (even for $N_b = 11$), so there are still some small finite-volume effects. Finally our error bars were only calculated from statistical error, the actual errors may be larger due to systematic errors.
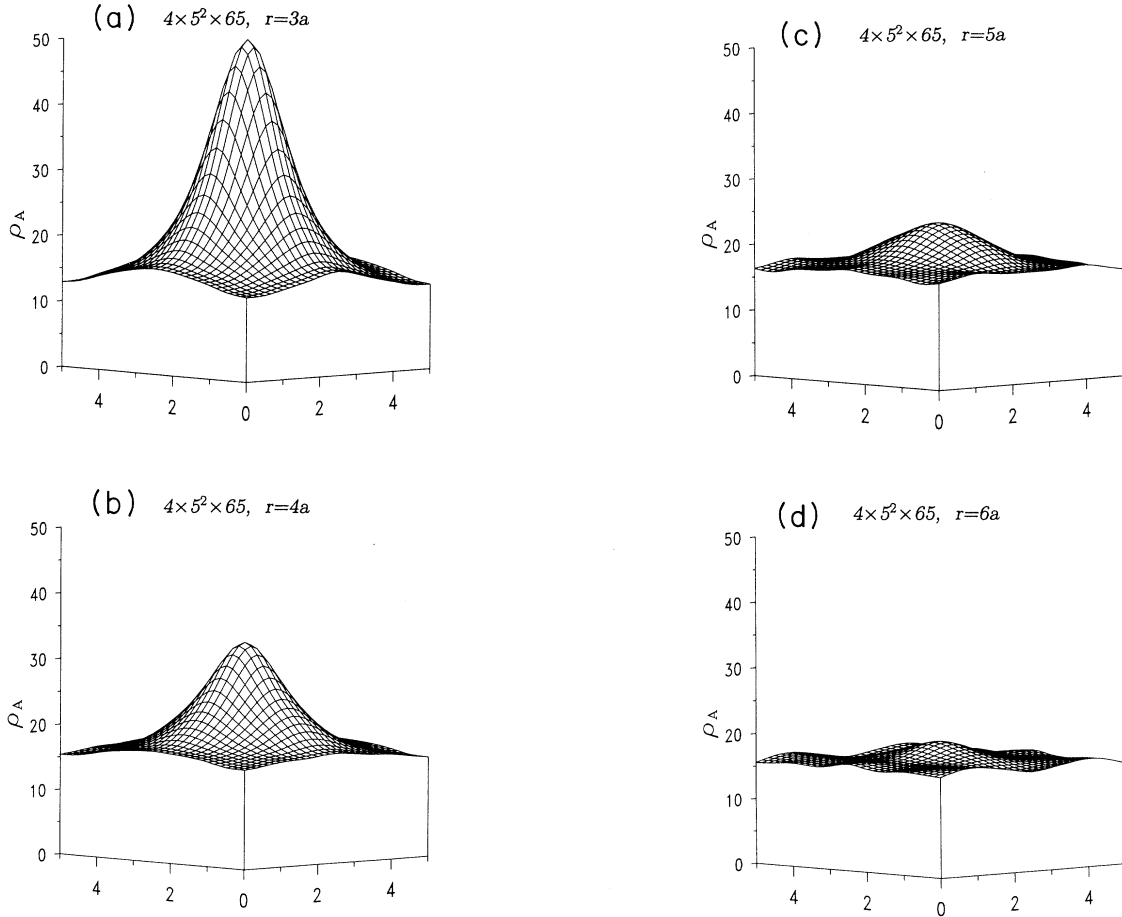

FIG. 3. The action density ρ_A flux distributions in the region $\beta > \beta_c$ on the plane midway between the $q\bar{q}$ sources of various separations (a) $r = 3a$, (b) $r = 4a$, (c) $r = 5a$, and (d) $r = 6a$. The flux data were measured on lattices $4 \times 5^2 \times 65$ with $\beta = 2.40$. The data are measured in the physical unit GeV/fm^3.

To see the behavior of the flux distributions changing with the $q\bar{q}$ separation r, in Fig. 3 we show the ρ_A distribution on the transverse plane for four different separations, $r = 3a$, $4a$, $5a$, and $6a$. The flux data were measured on the lattice $4 \times 5^2 \times 65$ with $\beta = 2.40$. From this figure one can see the peak values of ρ_A decrease rapidly with the increase of r. At large r (i.e., $r = 6a$) the peak of ρ_A almost vanishes, the flux density on the plane approaches a uniform distribution.

We then calculated the center slice energy σ_E and action σ_A from our flux data, which are the energy and action stored in the transverse slice of unit thickness midway between the $q\bar{q}$ pair. The results are shown in Fig. 4. In this figure we plot the behaviors of σ_E versus r and σ_A versus r, respectively, for $\beta = 2.36$. This shows that for N_b small σ_E and σ_A do not decrease to zero as r increases. However, for N_b large (e.g., $N_b = 9$, 11), σ_E and σ_A decrease rapidly with r and become very small at large $q\bar{q}$ separations (i.e., $r = 6a$).

B. Analysis of finite-volume effects for cases with $\beta > \beta_c$

To see how the finite-volume effects influence $q\bar{q}$ flux distributions in a finite box, let us consider an electrostatic charge pair $+e$, $-e$ enclosed in a similar long rectangular box such as that of Fig. 1. The interaction between charges is the Coulomb interaction $V(r) \sim 1/r$. As the charge separation r becomes very large, i.e., $r/N_b a \to \infty$, one can assume the electric field $\mathcal{E}$ on the middle transverse plane is uniform, and can be written as

$$\mathcal{E} = \frac{\Phi}{(N_b a)^2}, \tag{15}$$

where Φ is electric flux through the transverse plane, which is a constant for the Coulomb interaction, and $(N_b a)$ is the transverse size of the box. So the total electric field energy on the transverse plane is

$$(\sigma_E)_C = \frac{1}{2}\mathcal{E}^2(N_b a)^2 \sim \frac{1}{(N_b a)^2}. \tag{16}$$

This shows that at large charge separations the center slice energy $(\sigma_E)_C$ decreases with the behavior $(N_b a)^{-2}$ as the transverse size N_b increases, and $(\sigma_E)_C$ vanishes as $N_b \to \infty$, where the label C denotes a Coulomb interaction.

Now let us return to the $q\bar{q}$ pair in the box with $\beta > \beta_c$. As we discussed in the above section, the system approaches the unconfined phase for large N_b. In this phase the $q\bar{q}$ interaction is a screened Coulomb interaction $V(r) \sim e^{-mr}/r$ with m the screening mass [12]. Then if the $q\bar{q}$ pair is put in a box such as that in Fig. 1, the flux Φ through the transverse plane is not a constant, but would decrease with r and N_b. So we expect that in this case the center slice energy σ_E for a $q\bar{q}$ pair would
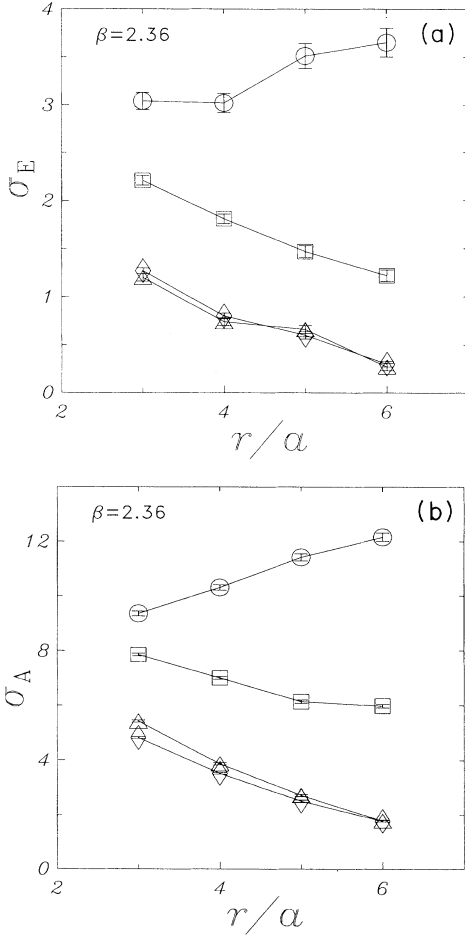

FIG. 4. The behavior of center slice energy σ_E and action σ_A vs the $q\bar{q}$ separation r in the region of $\beta > \beta_c$, (a) σ_E vs r, (b) σ_A vs r. The data were measured on lattices $4 \times N_b^2 \times 65$ with $\beta = 2.36$ for various spatial sizes, $N_b = 5$ (circles), $N_b = 7$ (squares), $N_b = 9$ (triangles), $N_b = 11$ (diamonds). The data are in the physical unit GeV/fm.
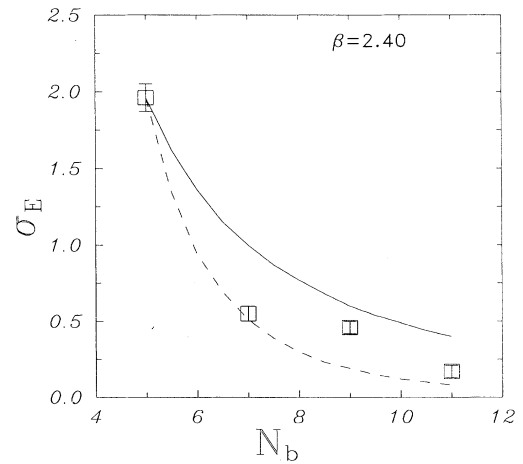

FIG. 5. The plot of σ_E in the region of $\beta > \beta_c$ vs the transverse size of lattices N_b at large $q\bar{q}$ separation $r = 6a$. The solid line is the Coulomb behavior $(N_b a)^{-2}$, the dashed line is the inverse quartic behavior $(N_b a)^{-4}$, both are normalized to the data at $N_b = 5$. The data were measured on lattices $4 \times N_b^2 \times 65$ with $N_b = 5$, 7, 9, 11, and $\beta = 2.40$.

decay faster with N_b than $(\sigma_E)_C$, which has the inverse square behavior, $(\sigma_E)_C \sim (N_b a)^{-2}$, for $r \to \infty$. In Fig. 5 we plot our σ_E data versus the transverse size N_b for large $q\bar{q}$ separation r. Our data are compared with the Coulomb behavior $(N_b a)^{-2}$ and for reference purposes the inverse quartic behavior $(N_b a)^{-4}$. The data were measured on lattices $4 \times N_b^2 \times 65$ with $N_b = 5, 7, 9, 11$ and $\beta = 2.40$.

From Fig. 5 one can see that for large r our σ_E data appear to decay faster with N_b than the Coulomb behavior $(N_b a)^{-2}$ as expected. This shows us that the $q\bar{q}$ interaction in the unconfined phase at least contains a term that decays faster than the Coulomb interaction, such as the screened Coulomb interaction, although the data are not good enough to determine the screening mass.

In conclusion, our flux data in the region of $\beta > \beta_c$ show that in the unconfined phase there is no string formation. For a small transverse size N_b, the finite-volume effects are large; the flux lines between a $q\bar{q}$ would be squeezed by side walls of the box significantly. This would result in a finite string tension.

C. Flux distributions with $\beta < \beta_c$

For $\beta < \beta_c$ the $q\bar{q}$ system approaches the confined phase as the volume becomes large ($N_b \to \infty$). We expect string formation would occur in this phase. To see this we need to study behaviors of the flux distributions as a function of the $q\bar{q}$ separation r.

In Fig. 6 we show the action density ρ_A distribution changing with the $q\bar{q}$ separation r. The flux data were measured on the lattice $4 \times 11^2 \times 65$ with $\beta = 2.25$. Since N_b is large (N_b=11) we deleted the margins of the transverse cross section of the lattice, as we did in Fig. 2. This figure should be compared with Fig. 3, which is for $\beta > \beta_c$. One can see Fig. 6 shows significantly different behavior from Fig. 3. In Fig. 6 the peak values of ρ_A on the plane approach a finite value as r becomes large. Even at large r (i.e., $r = 6a$) this peak still exists. However, in Fig. 3 the peak of the ρ_A distribution almost disappears at $r = 6a$. So the flux distribution in Fig. 6 implies that intrinsic string formation occurs in the region of $\beta < \beta_c$. This is not due to finite-volume
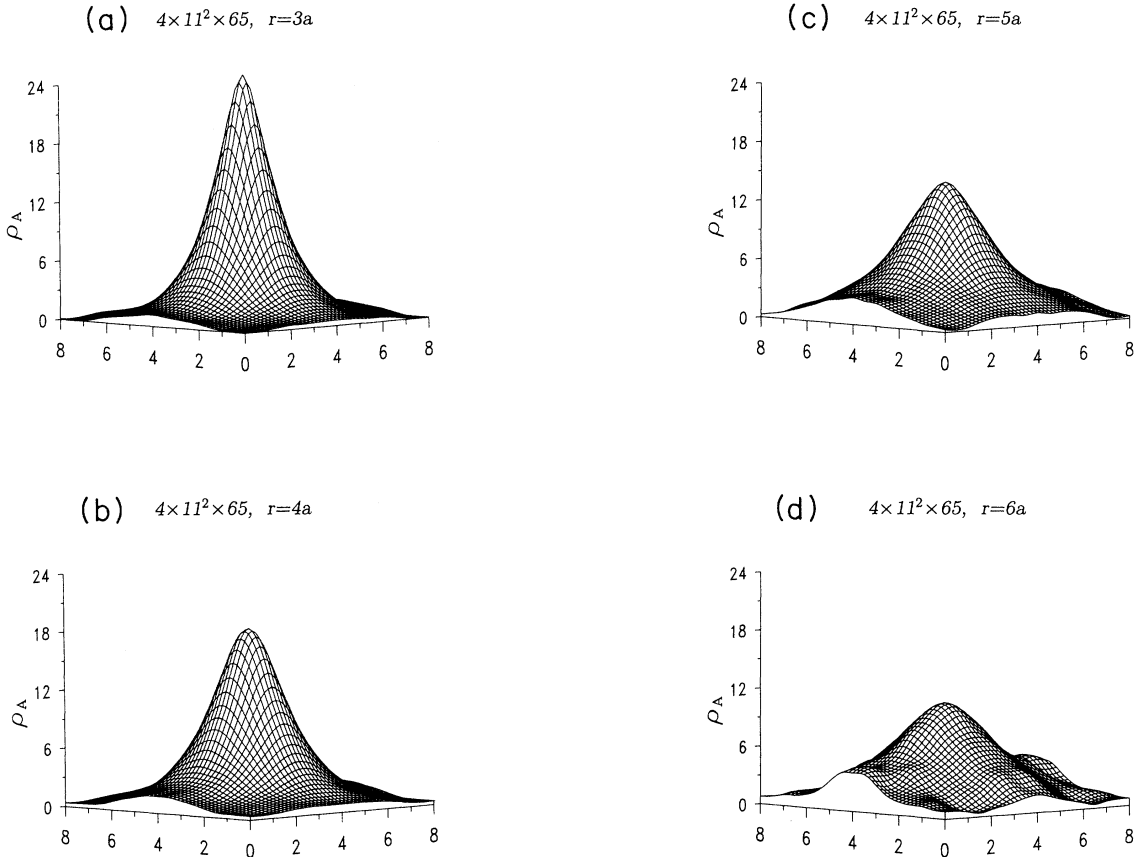

FIG. 6. The action density ρ_A flux distributions in the region of $\beta < \beta_c$ on the plane midway between the $q\bar{q}$ sources of various separations (a) $r = 3a$, (b) $r = 4a$, (c) $r = 5a$, and (d) $r = 6a$. The flux data were measured on lattices $4 \times 11^2 \times 65$ with $\beta = 2.25$. The data are measured in the physical unit GeV/fm^3.

effects because these effects are small at large volumes (i.e., N_b=9, 11), as we discussed in Fig. 2 and Table II.

We also calculated the center slice energy and action σ_E, σ_A from our flux data in the region $\beta < \beta_c$. If string formation occurs in the confined phase, for N_b large both σ_E and σ_A should approach some finite nonzero constants when $r \to \infty$. In Fig. 7 we plot the behaviors of σ_E versus r and σ_A versus r, respectively, for $\beta = 2.28$. The data were measured on lattices of various spatial sizes N_b=5, 7, 9, 11. From this figure one can see that in all cases σ_E and σ_A do not decrease with r. For each fixed N_b the values of σ_E and σ_A are almost constant as r increases. Further, for large N_b ($N_b = 9$, 11), where finite-volume effects are small, both σ_E and σ_A keep as finite nonzero constants as r becomes large. This behavior is totally different from that of Fig. 4, which is in the region of $\beta > \beta_c$. So Fig. 7 also implies that string formation occurs. In this figure we also notice that fluctuations of
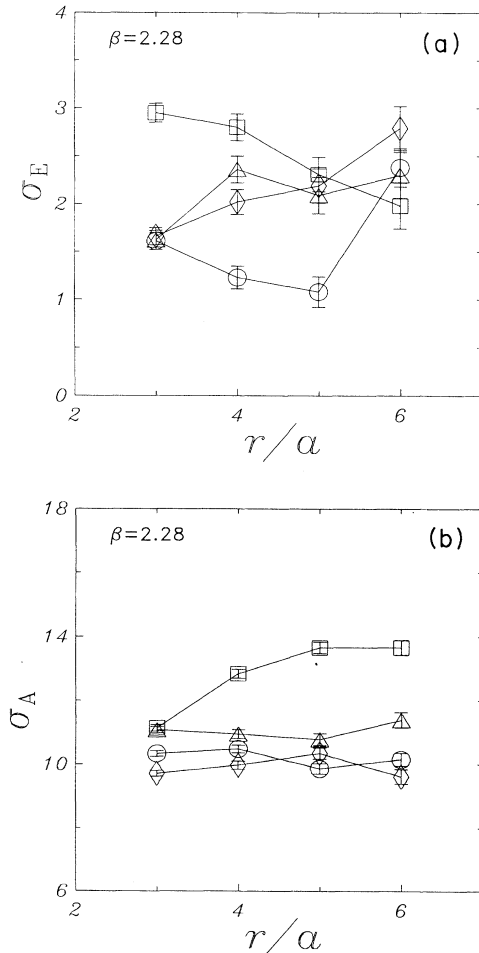
the data are large compared to the unconfined data. This is a typical behavior because confinement corresponds to disorder.

In conclusion, our flux data in the region of $\beta < \beta_c$ provide evidence for intrinsic string formation in the confined phase. This string formation is not due to finite-volume effects because these effects are small as the volume becomes large (i.e., $N_b = 9, 11$).

IV. SU(2) GAUGE THEORY IN FINITE VOLUMES AT $T_B \approx 0$

As we discussed in Sec. I, we have two ways to interpret the LGT calculations. One way is to identify the shortest extent N_a of lattices to be the temporal size. This is a convenient way to study the LGT system. In previous sections we have discussed our calculation results in this way. However, to compare with analytical results in finite volumes at zero temperature, one can use another way to interpret LGT results, that is, the longest extent N_c of lattices is chosen as the time direction, so that the temperature is as low as possible. In this case Polyakov loops closed in the N_a (or N_b) direction are no longer viewed as quark sources; they are considered to be spatial operators. Quantities such as the glueball mass and string tension can be calculated from Polyakov loop correlations along the time direction (N_c). No matter which way we choose, quantities calculated in LGT are the same; the mathematics of the two ways are equivalent. In this section we shall look at the system in terms of this second interpretation, and reinterpret the results of previous sections.

If we choose N_c as the time direction, we are studying SU(2) gauge theory in the volume $U = N_a N_b^2 a^3$ at near zero temperature $T_B = 1/N_c a$, because N_c is large. For convenience, instead of z_g defined in Eq. (1), we shall use another parameter, $z_\kappa = \sqrt{\kappa} L = \sqrt{\kappa} N_b a$, to characterize the physical size of the volume [4], where κ is the string tension measured by two Polyakov loops closed in N_a with correlations measured along N_c. This corresponds to κ_t of Ref. [4]. Koller and van Baal used z_g in their analytical calculations [3], so that they could easily compare with Monte Carlo results. Berg and Billoire used both z_g and z_κ parameters and other z parameters in analyses of their LGT Monte Carlo data for convenience [4]. The parameter z_κ is equivalent to z_g. For example, from the data of Ref. [4] one can see that $z_g \approx 1$ corresponds to $z_\kappa \approx 0.24$, and $z_g \approx 5$ corresponds to $z_\kappa \approx 1.3$. In Table III we show the correspondence of z_g and z_κ.

FIG. 7. The behavior of center slice energy σ_E and action σ_A vs the $q\bar{q}$ separation r in the region of $\beta < \beta_c$, (a) σ_E vs r, (b) σ_A vs r. The data were measured on lattices $4 \times N_b^2 \times 65$ with $\beta = 2.28$ for various spatial sizes, $N_b = 5$ (circles), $N_b = 7$ (squares), $N_b = 9$ (triangles), $N_b = 11$ (diamonds). The data are in the physical unit GeV/fm.

TABLE III. The correspondence of the two parameters $z_g = m(0^+)N_b a$ and $z_\kappa = \sqrt{\kappa} N_b a$, which are obtained from data in Ref. [4].

Small volume	Intermediate volume	Large volume
$z_g < 1$	$1 < z_g < 5$	$z_g > 5$
$z_\kappa < 0.24$	$0.24 < z_\kappa < 1.3$	$z_\kappa > 1.3$

TABLE IV. The values of the string tension data and z_κ on lattices of size $4 \times N_b^2 \times 64$ with $N_b = 4$, 6, 8 and $\beta = 2.36$, 2.38, and 2.41. The data are quoted from Ref. [4].

| | N_b | $4 \times N_b^2 \times 64$ | | |
		4	6	8
$\beta = 2.36$	$\sqrt{\kappa}a$	0.2475 (18)	0.1593 (39)	0.1091 (39)
	$z_\kappa = N_b\sqrt{\kappa}a$	0.99 (1)	0.96 (2)	0.87 (3)
$\beta = 2.38$	$\sqrt{\kappa}a$	0.2424 (23)	0.1357 (44)	0.0732 (81)
	$z_\kappa = N_b\sqrt{\kappa}a$	0.97 (1)	0.81 (4)	0.59 (6)
$\beta = 2.41$	$\sqrt{\kappa}a$	0.2264 (14)	0.1314 (51)	
	$z_\kappa = N_b\sqrt{\kappa}a$	0.91 (1)	0.79 (3)	

A. Results in intermediate volumes ($0.24 < z_\kappa < 1.3$)

In this part we will show that our lattices with $\beta > \beta_c$ belong to the intermediate volume region. Since in this region our string tension data have large error bars, we just simply use the string tension data of Ref. [4] to show that our lattices with $\beta > \beta_c$ satisfy $0.24 < z_\kappa < 1.3$. The data of Ref. [4] are given in Table IV, which have high statistical accuracies.

From Table IV we can see the values of string tension $\sqrt{\kappa}a$ and the parameter z_κ decrease with the increase of N_b and β. Our data were measured on lattices of the size $4 \times N_b^2 \times 65$ with $N_b = 5$, 7, 9, 11 and $\beta = 2.36$ and 2.40, which are similar to the lattices in Table IV. We can estimate our string tension and values of z_κ from Table IV. For example, the estimated string tension for the lattice $4 \times 5^2 \times 65$ with $\beta = 2.36$ could be interpolated from the string tension measured on lattices $4 \times N_b^2 \times 64$ with $N_b = 4$, 6 and $\beta = 2.36$. From Table IV one can see that for $N_b = 5$ the string tension satisfies $0.1593 < \sqrt{\kappa}a < 0.2475$, and $0.80 < z_\kappa = \sqrt{\kappa}aN_b < 1.24$, which is in the intermediate volume region, $0.24 < z_\kappa < 1.3$, as shown in Table III. By comparing our lattices with Table IV in this way, we find that our lattices with $\beta = 2.36$ and 2.40 for $N_b = 5$, 7, 9, 11 are all in the intermediate volume region, with the *box temperature* approaching zero, i.e., $T_B \to 0$.

As we discussed in Sec. III, for $\beta > \beta_c$ there is no intrinsic string formation. However, since finite-volume effects are large when the transverse size N_b is small, this results in the observed string tension in these cases. As N_b becomes larger, finite-volume effects becomes smaller, the string tension becomes smaller. This is confirmed in Table IV. Since the lattices with $\beta > \beta_c$ in our study all belong to the intermediate volume region, in these cases we find there is no intrinsic string formation, and the string tension is due to finite-volume effects. In general, we expect that the results apply to the whole intermediate volume region in the zero-temperature limit ($T_B \to 0$).

B. Results in large volumes ($z_\kappa > 1.3$)

For $\beta < \beta_c$ we can easily extract the string tension, which is given in Table V. In this table we also show

the values of z_κ for lattices with $\beta < \beta_c$. We can see that most lattices listed in Table V satisfy $z_\kappa > 1.3$, with one case in the critical region, $z_\kappa \approx 1.3$ for $\beta = 2.28$ and $N_b = 5$. From Table III we know that lattices satisfying the condition, $z_\kappa > 1.3$, belong to the large volume region in the zero-temperature limit ($T_B \to 0$). So our lattices with $\beta < \beta_c$, as listed in Table V, are in this region.

As we discussed in Sec. III C, a system with $\beta < \beta_c$ is in the confined phase in the infinite volume limit. In this case we have shown that intrinsic string formation occurs. As the transverse size N_b is made small (e.g., $N_b = 5$), we also observed some finite-volume effects; however, it does not change the nature of $q\bar{q}$ confinement. We have shown that the lattices with $\beta < \beta_c$ in our study all belong to the large volume region in the zero-temperature limit ($T_B \to 0$). From our study we have found evidence for intrinsic string formation in these cases, which is not due to finite-volume effects. We expect that the intrinsic string formation occurs in the whole large volume region.

V. SUMMARY

We used two ways to interpret the LGT results calculated on lattices $N_a \times N_b^2 \times N_c$ with the geometry $N_a \leq N_b \ll N_c$. First, we chose the convenient way to interpret our data, by identifying N_a to be the time

TABLE V. The string tension data κ and the values of the z_κ parameter on lattices of the size $4 \times N_b^2 \times 65$ with $N_b = 5$, 7, 9, 11 and $\beta = 2.25$ and 2.28.

N_b	β	$4 \times N_b^2 \times 65$ $\sqrt{\kappa}a$	$z_\kappa = N_b\sqrt{\kappa}a$
5	2.25	0.300 (22)	1.5 (1)
	2.28	0.251 (34)	1.3 (2)
7	2.25	0.288 (31)	2.2 (2)
	2.28	0.258 (31)	1.8 (2)
9	2.25	0.262 (84)	2.4 (8)
	2.28	0.226 (67)	2.0 (6)
11	2.25	0.307 (48)	3.4 (5)
	2.28	0.232 (64)	2.6 (7)

direction we can study the system at finite temperatures $(T_p = 1/N_a a)$ in the volume $V = N_b^2 N_c a^3$. We analyzed the flux distributions of a $q\bar{q}$ pair in terms of this interpretation. If we choose N_c to be the time direction we can study the system at near zero temperature $(T_B = 1/N_c a)$ in the volume $U = N_a N_b^2 a^3$. We find that for $\beta > \beta_c$ there is no intrinsic string formation. Our lattices with $\beta > \beta_c$ belong to the intermediate volume region. We then established that the origin of the string tension measured by Berg and Billoire [4] in this region is related to finite sizes of the lattice. For $\beta < \beta_c$ we find clear signals for intrinsic string formation. Our lattices with $\beta < \beta_c$ are in the large volume region, but near the borderline of intermediate volumes and large volumes. This is just beyond the volume region investigated by Berg and Billoire.

Another remark on string formation is that for higher units of 't Hooft electric flux one expects that string formation predicts the relation [4],

$$E_n = \sqrt{n}E_1 \qquad (n = 1, 2, \ldots), \tag{17}$$

where E_n is the energy of the n unit flux. However, both analytical results [3] and LGT calculations [4] produce a different behavior in the intermediate volume region,

$$E_n \approx nE_1, \tag{18}$$

where $n = 1, 2, 3$ for SU(2). Even in the large volume region some Monte Carlo data of Ref. [4] still show the behavior of Eq. (18). We speculate that Eq. (17) may be due to lattice artifacts since the origin of $\sqrt{2}$ and $\sqrt{3}$ in this equation are for the planar diagonal and volume diagonal on lattices.

Our study supplements the global study of Berg and Billoire [4], and provides evidence that string formation does not occur in intermediate volumes, but occurs in large volumes. To verify Eq. (17) or (18) we need to measure the energy E_n of higher unit flux in the large volume region.

ACKNOWLEDGMENTS

[1] M. Lüscher, Nucl. Phys. **B219**, 233 (1983).

[2] M. Lüscher and G. Munster, Nucl. Phys. **B232**, 445 (1984).

[3] J. Koller and P. van Baal, Nucl. Phys. **B302**, 1 (1988).

[4] B.A. Berg and A.H. Billoire, Phys. Rev. D **40**, 550 (1989).

[5] P. Weisz and V. Ziemann, Nucl. Phys. **B284**, 157 (1987).

[6] C.W. Bernard, Phys. Rev. D **9**, 3312 (1974); L. Dolan and R. Jackiw, *ibid.* **9**, 3320 (1974).

[7] J. Wosiek and R.W. Haymaker, Phys. Rev. D **36**, 3297 (1987); R. Sommer, Nucl. Phys. **B306**, 181 (1988).

[8] R.W. Haymaker and J. Wosiek, Phys. Rev. D **43**, 2676 (1991);

[9] Y. Peng and R.W. Haymaker, LSU report (unpublished).

[10] A.M. Polyakov, Phys. Lett. **72B**, 477 (1978); L. Susskind, Phys. Rev. D **20**, 2610 (1979).

[11] J. Engels, J. Fingberg, and M. Weber, Nucl. Phys. **B332**, 737 (1990).

[12] J. Kuti, J. Polonyi, and K. Szlachanyi, Phys. Lett. **98B**, 199 (1981).